

NEOCORTICAL CELL TYPE CLASSIFICATION FROM ELECTROPHYSIOLOGY RECORDINGS USING DEEP NEURAL NETWORKS

Anonymous authors

Paper under double-blind review

ABSTRACT

Understanding the neural code requires identifying different functional units involved in the neural circuits. One way to identify these functional units is to solve a neuron type classification problem. For decades, current-clamp electrophysiology recordings have provided the means to classify the neurons based on subtle differences in action potential shapes and spiking patterns. However, significant variations in neuronal type definitions, classification pipelines, and intrinsic variability in the neuronal activities make unambiguous determination of neuron type challenging. Previous solutions to this electrophysiology-based cell type classification problem consisted of dimensionality reduction juxtaposed with clustering using hand-crafted action potential features. Recent discoveries have allowed genetics-based cell-type classifications, which have fewer ambiguities, but they are less practical in vivo and have even lower throughput. Leveraging the unprecedented ground truth data published in the Allen Institute Cell Types Database, which contains anatomical, genetic, and electrophysiological characterizations of neurons in the mouse neocortex, we construct a robust and efficient convolutional neural network (CNN) that successfully classifies neurons according to their genetic label or broad type (excitatory or inhibitory) solely using current-clamp electrophysiology recordings. The CNN is configured as a multiple-input single-output network consisting of three subnetworks that take in the raw time series electrophysiology recording as well as the real and imaginary components of its Fourier coefficients. Our single pipeline method is fast and streamlined while simultaneously outperforming a previous method. Furthermore, our method achieves classification with more classes using only a single current-clamp time series trace as the input. This end-to-end convolutional neural network-based classification method removes the need for hand-crafted features, specific knowledge, or human intervention for quick identification of the neocortical cell type with high accuracy, enabling interpretation of experimental data in a bias-free manner and understanding of a much broader scientific context.

1 INTRODUCTION

The neuronal type classification problem has been present in neuroscience since Ramón y Cajal’s presentation of the neuron doctrine, which highlighted the ample diversity of neurons. Neuroscientists hypothesized that morphological differences play a functional role in neural circuits. This intuition was extended to the investigation of the differences in neuronal activity with the appearance of the current clamp technique, which allowed observations of various action potential shapes and patterns in neurons.

Features such as action potential (AP) threshold and frequency, full width at half maximum (FWHM) of an action potential (AP width), or afterhyperpolarization values and their common ratios in subsequent action potentials in a train, which are easily distinguishable by a person, aimed to describe the differences among the observed variabilities in neuronal activities. Although no two neurons have the same activity, these hand-crafted features were used to define the electrophysiological types of neurons (Beierlein et al., 2003; Nowak et al., 2008). Due to the intrinsic neuron-to-neuron variabil-

ities and the lack of established features that definitively separate neuron types, no single pipeline is sufficient enough for unambiguous classification.

Several electrophysiology-based classification pipelines including methods that consider more features and ones that focus only on a single neuronal subpopulation coexist today (Petilla Interneuron Nomenclature Group; PING and others, 2008; Markram et al., 2004). Previous solutions to this cell type classification problem were comprised of a combination of dimensionality reduction and clustering using calculated action potential features and cell morphology. These approaches suffered in classification accuracy as they relied on AP shape, spiking pattern, or cell shape parameters that span a continuous feature space, which often do not have clear separation boundaries.

In addition to the aforementioned classification method based on morphology and electrophysiology, one based on the genetic makeup of neurons appeared recently in systems neuroscience (Tasic et al., 2018). A vast majority of neurons can be clustered according to their genetic encoding characteristic of the group proteins. This gene-based consideration of neuron type allows a less ambiguous classification pipeline. The most commonly used genetic types of neurons are neuron-derived neurotrophic factor (Ndnf), parvalbumin (Pvalb), somatostatin (Sst), and vasoactive intestinal peptide (Vip) interneurons, and excitatory (Exc) neurons that are predominantly pyramidal cells.

Furthermore, the emergence of genetically modified transgenic lines of animals, where cells of a selected genetic type can be marked by a fluorophore, enabled studies relating electrophysiological neuronal activity to the genetic type of neurons (Taniguchi et al., 2011). Attempts to characterize the electrophysiological features of specific genetic types of neurons revealed that the majority of Pvalb interneurons correspond to Fast Spiking (FS) electrophysiological cell type, but both Vip and Sst interneurons as well as excitatory neurons can appear as Regular Spiking (RS) or Low Threshold Spiking (LTS) types (Contreras, 2004). Therefore, we can conclude that there does not exist a clear mapping from one classification scheme to another, partially due to existing methods' low throughput and differences in definitions and experimental pipelines.

To address the challenges presented by the above neuron type classification problem and to improve on the existing classification pipeline architectures, a robust and efficient convolutional neural network (CNN) that successfully classifies neurons according to their genetic label or broad type (excitatory or inhibitory) solely using short snippets of current-clamp electrophysiology recordings has been developed. The method presented in this paper relies on the ground truth data published in the Allen Institute Cell Types Database, which contains anatomical and morphological descriptions, genetic types, and electrophysiology features of thousands of neurons in the mouse neocortex (Gouwens et al., 2019). We use this open access database, which is one of the flagship initiatives of the Allen Institute for Brain Science, to obtain the genetic type label of a given neuron, bypassing supervised definitions of all signal features. The following sections detail the related state-of-the-art methods, the specifications of our novel deep neural network-based neuron type classification method, as well as the results obtained using our custom CNN architecture.

2 RELATED WORK

Gouwens et al. (2019) built and made publicly available the Allen Institute Cell Types Database. From this database, 17 electrophysiological, 38 morphological, and 46 morpho-electric neuron types were identified using a custom classification pipeline. The authors employed biocytin-based neuronal reconstruction to extract morphological features and used raw current-clamp electrophysiology recordings of cells from the mouse visual cortex *in vitro* as inputs for electrophysiological features. After computing handcrafted single action potential features including action potential height, threshold, upstroke speed, and downstroke speed, as well as features corresponding to action potential trains, such as interspike intervals and spiking frequency, principal component analysis and t-distributed stochastic neighbor embedding techniques were applied to project the high-dimensional electrophysiological feature space into two dimensions. With clustering, the authors were able to identify 17 electrophysiological neuron types, 4 of which were classified as excitatory subtypes and 13 of which were inhibitory. The 13 inhibitory subtypes were further mapped to the four inhibitory interneuron types based on their genetic tags: Sst, Vip, Pvalb, and Ndnf.

Ghaderi et al. (2018) successfully developed a semi-supervised technique to classify neuron types using limited in vivo electrophysiology recordings data. The authors considered only 3 types of neurons: excitatory pyramidal (Pyr) cells, parvalbumin positive (Pvalb) interneurons, and somatostatin positive (Sst) interneurons from layer 2/3 of the mouse primary visual cortex. After extracting single spikes, they extracted discriminative action potential features by computing the Discrete Cosine Transform of the recorded electrophysiology traces. Principal component analysis and fuzzy c-means clustering were then performed, and neurons were subsequently classified using a minimum distance classifier. The authors achieved accuracies of 91.59 ± 1.69 , 97.47 ± 0.67 , and 89.06 ± 1.99 for Pvalb, Pyr, and Sst, respectively, which yielded an overall accuracy of $92.67 \pm 0.54\%$. This classification algorithm pipeline was further applied to the in vitro data from the Allen Institute Cell Types Database containing Pvalb, Sst, 5HT3a, and Vip genetic types. Testing on a dataset comprised of a pool of 50 neurons where multiple electrophysiology traces have been recorded for each neuron, the authors achieved accuracies of $93.57 \pm 0.59\%$, $89.15 \pm 0.63\%$, $81.69 \pm 0.56\%$, $79.23 \pm 1.38\%$, and $77.02 \pm 0.91\%$ for Pvalb, Sst, Vip, 5HT3a, and Pyr, respectively.

3 METHODS

In this paper, we present a neuron type classification technique based on a simple convolutional neural network (CNN) architecture. Using in vitro current-clamp electrophysiology recording traces of neurons in the mouse neocortex, the CNN is configured as a multiple-input single-output network consisting of three subnetworks. The first subnetwork takes in a portion of the raw time series recording that is 50 ms in duration and contains at least one action potential. The real and imaginary components of a trace’s Fourier coefficients are fed into the second and third subnetworks of the CNN, respectively. A graphical representation of the CNN architecture is shown in Figure 3.

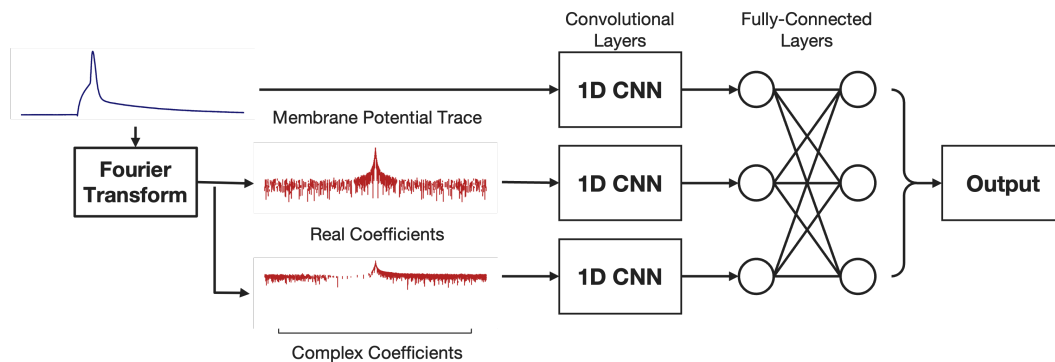


Figure 1: Graphical representation of the triple-input CNN architecture.

3.1 DATASET

We use data collected from 1947 cells in the Allen Institute Cell Types Database (Gouwens et al., 2019). Of these, we omitted 81 cells containing only morphological features and lacking electrophysiology recordings, and only the remaining 1866 cells containing electrophysiology recordings were used to build our training, validation, and test sets. Every one of these 1866 cells was obtained from transgenic animal lines, and thus is associated with a genetic label (Exc, Ndnf, Vip, Sst, and Pvalb). Each neuron contains approximately 50 electrophysiology trace recordings that are responses to multiple current-clamp stimuli including short square, long square, ramp, and noise. Of these traces, we only considered responses to the short square stimulus, which are 3 ms in duration, which is just long enough to induce a single action potential. Each of these recordings is collected at either 200 kHz or 50 kHz sampling rate. Because each neuron is recorded at a different stimulus level, we only consider the traces that contain an action potential.

To obtain the most useful information about the neuron type being assessed, the type of classification task that our architecture solves can be dictated by the needs of a neurophysiologist. One task is to distinguish neuronal activity coming from an excitatory (Exc) or an inhibitory (Inh) neuron.

162 This task is less informative, but provides explanation useful for analyzing electrophysiological
163 recordings. The more interesting task is to discriminate among the 5 genetic types (Pvalb, Sst, Vip,
164 and Ndnf inhibitory interneuron types and Exc neuron type), which constitute the broader excitatory
165 and inhibitory categories. Reliable and accurate classification among the 5 genetic types is highly
166 valuable to the neuroscience community. We train our network to perform the two aforementioned
167 tasks.

168 3.2 PREPROCESSING

169 One of the main objectives of our approach is to remove as much supervised overhead in the data
170 processing stage of the neuron type classification pipeline as possible. The only preprocessing steps
171 we perform on the raw time series data is removing excess temporal portions of recordings that do
172 not provide useful information. We are only interested in the portion of the recording containing an
173 action potential, so only 50 ms of recording, 25 ms before and 25 ms after the onset of the short
174 square stimulus, was considered. The 25 ms of pre- and post-stimulus time duration was chosen
175 to ensure that potential discriminative features that may be present before or after the onset of the
176 stimulus would be captured by the representation learning performed by our convolutional neural
177 network. The 25 ms of post-stimulus time guarantees that a single action potential has returned to
178 its resting membrane potential after depolarization and hyperpolarization.

179 We also take the fast Fourier transform of these 50 ms time series traces. The real and imaginary
180 components of the resulting Fourier coefficients, in addition to the corresponding time series traces,
181 are used as inputs to the subnetworks of our convolutional neural network architecture.

182 For model selection and performance, we divide the aforementioned dataset collection from the
183 Allen Institute Cell Types Database based on the unique cell identification numbers. The ratio
184 between the training and validation sets was fixed at 8:2. Once the best generalized performing
185 model was identified, we independently split the dataset again based on the unique cell identification
186 numbers. Eighty percent of the data were reserved for training and the remaining 20% were set
187 aside as the test set data. The test set was further split as follows: 80% test and 20% validation. The
188 validation set was used to tune the network hyperparameters. This dataset separation by cell prevents
189 overfitting, and provides both significant advantage and improvement to the existing methods. Due
190 to natural cell-to-cell variations, basic action potential features like resting membrane potential can
191 vary considerably among cells of the same genetic type. We therefore use and report the maximum
192 validation accuracy we obtain over 100 epochs.

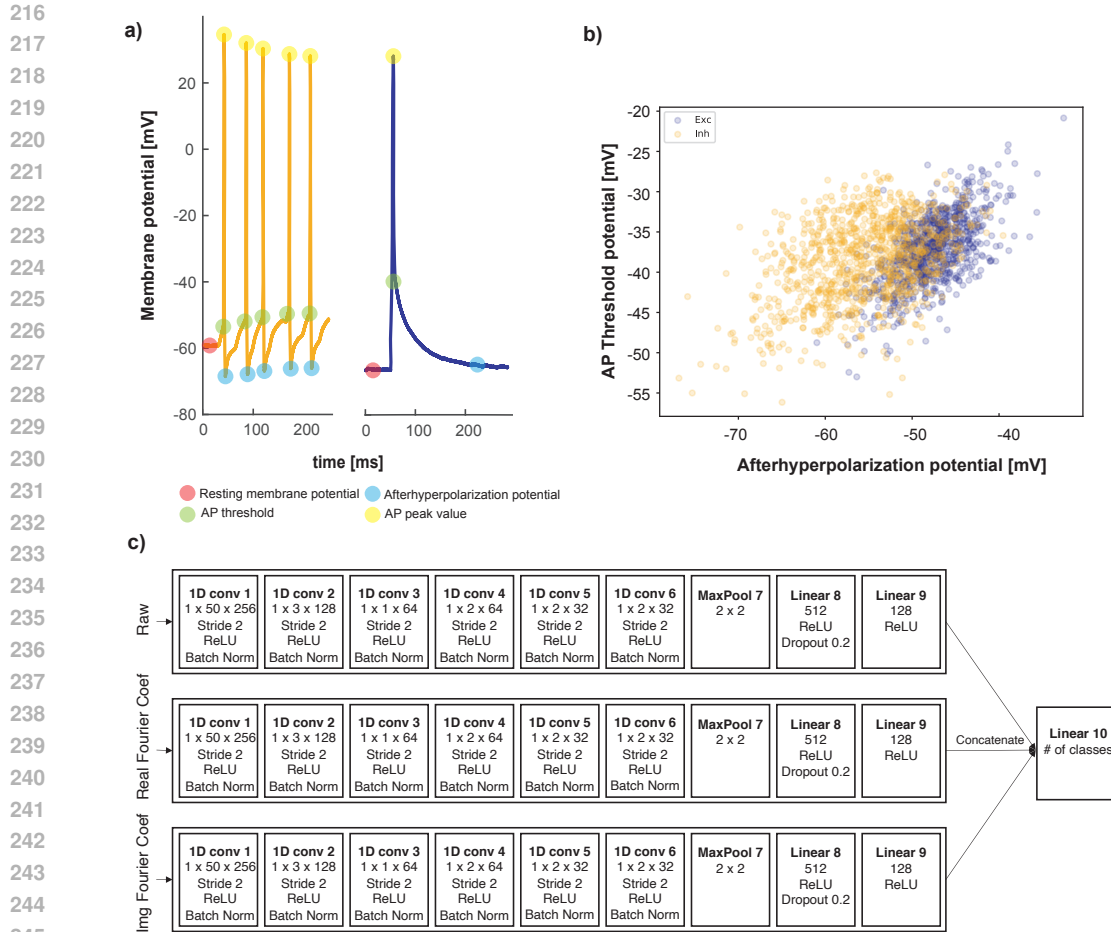
193 3.3 NETWORK ARCHITECTURE

194 We use a multiple-input single-output convolutional neural network (CNN) for training. To remove
195 the need for handcrafted features, our deep neural network uses a one-dimensional convolutional
196 neural network as a feature encoder and employs dense layers to output class predictions. The
197 standard one-dimensional CNN encoder is implemented using PyTorch. The encoder contains 6
198 convolutional layers, and each layer is passed through a Rectified Linear Unit (ReLU) activation
199 function. Batch normalization introduced by Ioffe & Szegedy (2015) is applied to each activated
200 layer. The exact specifications of each layer is shown in c) of Figure 3.3.

201 For training, we employ the Adam optimizer—with the learning rate set to 10^{-3} and the ℓ_2 regular-
202 ization parameter set to 10^{-5} —to minimize the cross entropy loss with sum reduction (Kingma &
203 Ba, 2014). The initial weights were randomly generated.

204 An 8:2 ratio training-validation data set split was used to select the optimal network model config-
205 uration. We first tried a single-input single-output configuration, where only the top stream in c) of
206 Figure 3.3 was used. This architecture resulted in a validation accuracy of 88.52% for classification
207 among the 5 genetic neuron types: Exc, Pvalb, Sst, Ndnf, and Vip; and a validation accuracy of
208 96.35% for classification between excitatory and inhibitory broad types.

209 We then tested using a dual-input single-output configuration. Features were trained independently
210 on each subnetwork and were concatenated at the final step for classification. Using only the real
211 component of the Fourier coefficients as input to the additional subnetwork resulted in validation
212 accuracies of 91.43% for classification among the 5 genetic neuron types, and 99.38% for classifi-
213 cation between excitatory and inhibitory broad types. Similarly, using only the complex component
214
215



253
254
255
256
257
258
259
260
261
262

of the Fourier coefficients resulted in validation accuracies of 89.13% for classification among the 5 genetic types, and 96.58% for classification between excitatory and inhibitory broad types.

263
264
265
266
267
268
269

Finally, we used a triple-input single-output configuration where the raw current-clamp electrophysiology recording time series trace as well as both the real and imaginary components of the Fourier coefficients are used as inputs. Features were also trained independently on each subnetwork and were concatenated at the final step for classification. This configuration was our best performing architecture, which resulted in validation accuracies of 92.05% for classification among the 5 genetic types and 98.10% for classification between excitatory and inhibitory broad types. This triple-input network architecture's ℓ_2 regularization hyperparameter was tuned to 10^{-5} .

3.4 TRANSFER LEARNING

One of the biggest challenges in decoding the neural circuit and in systems neuroscience in general is obtaining sufficient amount of data for each neuron type. Supervised learning requires a large number of sample data points to train efficient classifiers. One of the main difficulties we encountered in this work was the problem of class imbalance present in the datasets. For example, there are many more data points from excitatory (466) and parvalbumin (241) cells than Ndnf (46), Sst (86), and Vip (45) cells in the 5 class validation set; and many more data points from excitatory (644)

and parvalbumin (260) cells than Ndnf (38), Sst (130), and Vip (72) cells in the 5 class test set. We attempt to solve this problem using transfer learning.

From the results of our triple-input single-output network, we can conclude that the 2 class classification task of identifying excitatory versus inhibitory cells achieves high accuracy. This observation inspired us to first train the model on the task it does well, and then conduct fine-tuning. We therefore trained the aforementioned CNN network for the 2 broad type (Exc and Inh) classification task first for 100 epochs. We then changed the task to the 5 genetic type (Exc, Pvalb, Sst, Ndnf, and Vip) classification using the network trained on the two broad type classification task. The network uses the same CNN weights from the 2 type classification task, but has an output layer changed to the 5 type classification task. Then, the updated network underwent fine-tuning on the 5 type classification task for 100 epochs.

The same Adam optimizer with the learning rate of 10^{-3} and ℓ_2 regularization parameter of 10^{-5} was used for training. In order to investigate the model’s ability to undergo fine-tuning on a limited number of data points, we subjected the network to endure fine-tuning on the following training-test data set split ratios: 3:7, 5:5, and 8:2. For the 5 class classification task, at the epoch corresponding to the highest validation accuracy, the computed test set precisions were 86.87%, 87.46%, and 89.22%, for the above three training-test set split ratios, respectively. Table 1 reports the details of the test set precision values of the above transfer learning.

Table 1: Transfer learning precision

Type\Training-Test Set Ratios	3:7	5:5	8:2
Exc	97.65	98.08	94.60
Ndnf	96.59	89.43	90.00
Pvalb	80.99	79.93	91.25
Sst	71.76	72.26	84.13
Vip	44.65	51.70	45.65
Weighted Avg	86.87	87.46	89.22

In addition, we fine-tuned the network on the 5 type classification task, used a 5 type classification validation set, selected the epoch with the highest validation accuracy, and evaluated a 2 class classification task’s test set accuracy. This particular network, having never observed this 2 class classification test set data during training, resulted in a test set accuracy of 98.30%.

Finally, we trained the network on the current-clamp electrophysiology recordings data sampled at 200 kHz. We then transferred the trained model to a task using 50 kHz recordings while keeping the input size constant. This resulted in action potential features being stretched or compressed to fit the new sampling rate. When comparing this transfer approach to a control experiment where a newly initialized network was trained from start on the 50 kHz sampling rate data, we observed that the transferred model required less data to achieve higher accuracy values, as shown by Figure 3.4.

This finding highlights an important advantage of our model. Collecting data at different sampling rates is expensive. We have demonstrated that our method is capable of rapidly adapting to data obtained from varying sampling rates. We can thus conclude that our method significantly reduces costs associated with data collection.

4 RESULTS

Our best performing triple-input single-output network architecture resulted in a test set weighted average precision of 89.76% for classification among the 5 genetic neuron types: excitatory (Exc), parvalbumin (Pvalb), somatostatin (Sst), neuron-derived neurotrophic factor (Ndnf), and vasoactive intestinal peptide (Vip) cells. This finalized network architecture resulted in a test set weighted average precision of 98.28% for classification between excitatory and inhibitory broad types. For both tasks, the individual classes’ precisions, recalls, and F_1 -scores are reported in Table 2.

In order to obtain a better understanding and aid interpretability of the triple-input CNN’s classification performance, we investigated which genetic type was outputted for every genetic type input in

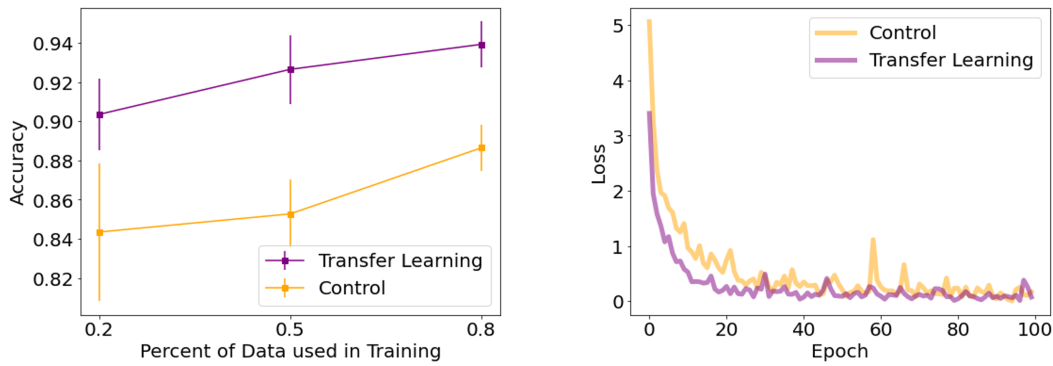


Figure 3: Performance comparison between models trained from start using data sampled at 50 kHz and models transferred from a 200 kHz sampling rate data task to a 50 kHz sampling rate data task. Transferred models achieve higher accuracy with less data, suggesting efficient learning and adaptation of action potential features across multiple sampling rates.

Table 2: Triple-input CNN precision

Type	Precision (%)	Recall (%)	F ₁ -Score (%)	Support
2 Class Validation Set				
Exc	98.78	98.78	98.78	490
Inh	98.52	98.52	98.52	406
Weighted Avg	98.66	98.66	98.66	896
2 Class Test Set				
Exc	97.28	99.51	98.38	611
Inh	99.42	96.80	98.10	532
Weighted Avg	98.28	98.25	98.25	1143
5 Class Validation Set				
Exc	96.27	99.79	98.00	466
Ndnf	84.62	95.65	89.80	46
Pvalb	99.17	98.76	98.96	241
Sst	88.24	87.21	87.72	86
Vip	87.50	46.67	60.87	45
Weighted Avg	95.23	95.36	94.94	884
5 Class Test Set				
Exc	94.93	98.76	96.80	644
Ndnf	57.63	89.47	70.10	38
Pvalb	93.08	93.08	93.08	260
Sst	77.54	82.31	79.85	130
Vip	70.59	16.67	26.97	72
Weighted Avg	89.76	90.12	88.75	1144

the 5 type classification task. The results are summarized in Table 3 and are represented graphically by the confusion matrix in Figure 4.

Although not necessarily a direct comparison of performance, Ghaderi et al. (2018) achieved an overall accuracy of 84.13% using the Allen Institute Cell Types Database containing Pyr (Exc), Pv (Pvalb), Sst, 5ht3a, and Vip cells. Using the Allen Institute Cell Types Database containing Pyr (Exc), Pv (Pvalb), Sst, Ndnf, and Vip cells, we achieved an overall accuracy of 90.12%.

Table 3: Classification accuracy results (%)

Output\Input	Sst	Vip	Ndnf	Pvalb	Exc
Sst	70.62	29.39	0.25	5.8	0.49
Vip	13.0	34.92	8.65	2.52	1.29
Ndnf	0.18	5.63	85.24	0.83	0.14
Pvalb	10.1	10.38	4.45	90.82	0.01
Exc	6.1	19.68	1.42	0.03	98.08

Table 4: For each cell type, both the correct classification rate as well as the rates for all misclassified genetic types are shown. Each column represents an input cell type, and each row indicates how frequently the CNN misclassified the input cell type as one of the other cell types.

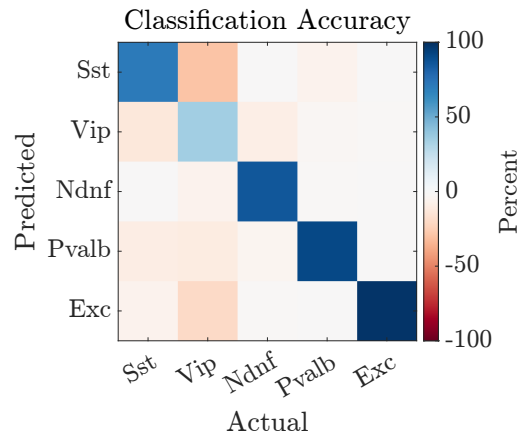


Figure 4: Confusion matrix of classification accuracy scores. Misclassification rates are represented by negative percentage values while correct classification rates are represented by positive percentage values.

For a more direct comparison of performance, we trained and applied the triple-input CNN on a partial dataset containing only Pv (Pvalb), Pyr (Exc), and Sst cells, and achieved the accuracies reported in Table 5. Our triple-input CNN was able to outperform the existing method on all fronts.

Table 5: Overall accuracy results comparison (%)

Class	Ghaderi et al. (2018)	Triple CNN
Pv	91.59	95.95
Pyr	97.47	98.29
Sst	89.06	90.00
Overall	92.67	96.89

5 CONCLUSION AND FUTURE WORK

We presented in this paper a solution to the neuron classification problem that avoids the use of existing imperfect, non-standardized, and cumbersome electrophysiological classification schemes. The triple-input CNN architecture described in this paper maps the pool of neurons into less ambiguous genetic classifications that is normally not widely accessible or practical in experimental pipelines. After training, our streamlined end-to-end convolutional neural network-based classification method does not require any domain specific knowledge or human intervention for quick identification of the

432 neuron’s cell type with high accuracy. The method presented in this paper provides an efficient and
433 standardized tool for the neuroscience community to use, thus enabling data analyses in a broader
434 scientific context. We also showed that the network architecture learns representations that suc-
435 cessfully distinguishes the neuron types, even when these features are not immediately recognizable
436 upon inspection as shown by the histograms of the time series data in the Appendix.

437 Although we achieved the state-of-the-art results, there exists a potential source of noise in our data.
438 The genetic labels we use in the training, validation, and test sets are currently based on the animal
439 type used to obtain the electrophysiology recording traces. The transgenic animal lines however are
440 not guaranteed to be accurate. It is known that some recordings obtained from a specified given
441 type will in fact belong to another genetic type (Hu et al., 2013). Quantifying how much error is
442 propagated from this potential noise source across all genetic types is of importance. Obtaining a
443 more accurate genetic labels from genetic sequencing data needs to be considered in the future.

444 Furthermore, we plan to augment our dataset with in vivo electrophysiology recordings, which are
445 inherently coupled with more background noise. Such an extension will be particularly beneficial
446 for rare, but highly valuable in vivo current-clamp recordings, which are often blind to cell type. By
447 removing the need for labor-intensive handcrafted feature computation, which traditionally requires
448 domain expertise, our approach can enhance reproducibility and lead to faster, less biased scientific
449 outcomes. Additionally, analyzing the network’s learned features may provide insights into which
450 neuronal activity patterns best define specific neuron types. It is widely assumed that genes encode
451 the ion channel repertoire that underlies electrophysiological activity (Nandi et al., 2022). Identifying
452 correlations or causal relationships between genetic and electrophysiological classifications
453 remains a key objective in neurophysiology. This pursuit aligns with Ramón y Cajal’s intuition that
454 neuron groups possess distinct, intrinsic properties.

455 As foundational models continue to shape the future of machine learning and neuroscience, our ap-
456 proach serves not only as a current solution, but also as a potential blueprint. It provides an encoding
457 mechanism for electrophysiology data that can seamlessly integrate into larger foundational models,
458 ultimately bridging the gap between cellular-level neural activity and large-scale neural representa-
459 tions.

460 REFERENCES

- 461 Michael Beierlein, Jay R Gibson, and Barry W Connors. Two dynamically distinct inhibitory net-
462 works in layer 4 of the neocortex. *Journal of neurophysiology*, 90(5):2987–3000, 2003.
- 463 Diego Contreras. Electrophysiological classes of neocortical neurons. *Neural Networks*, 17(5-6):
464 633–646, 2004.
- 465 Parviz Ghaderi, Hamid Reza Marateb, and Mir-Shahram Safari. Electrophysiological profiling of
466 neocortical neural subtypes: a semi-supervised method applied to in vivo whole-cell patch-clamp
467 data. *Frontiers in neuroscience*, 12:823, 2018.
- 468 Nathan W Gouwens, Staci A Sorensen, Jim Berg, Changkyu Lee, Tim Jarsky, Jonathan Ting, Su-
469 san M Sunkin, David Feng, Costas A Anastassiou, Eliza Barkan, et al. Classification of electro-
470 physiological and morphological neuron types in the mouse visual cortex. *Nature neuroscience*,
471 22(7):1182–1195, 2019.
- 472 Hang Hu, John Z Cavendish, and Ariel Agmon. Not all that glitters is gold: off-target recombination
473 in the somatostatin–ires-cre mouse line labels a subset of fast-spiking interneurons. *Frontiers in*
474 *neural circuits*, 7:195, 2013.
- 475 Sergey Ioffe and Christian Szegedy. Batch normalization: Accelerating deep network training by
476 reducing internal covariate shift. In *International conference on machine learning*, pp. 448–456.
477 PMLR, 2015.
- 478 Diederik P Kingma and Jimmy Ba. Adam: A method for stochastic optimization. *arXiv preprint*
479 *arXiv:1412.6980*, 2014.
- 480 Henry Markram, Maria Toledo-Rodriguez, Yun Wang, Anirudh Gupta, Gilad Silberberg, and Caizhi
481 Wu. Interneurons of the neocortical inhibitory system. *Nature reviews neuroscience*, 5(10):793–
482 807, 2004.

486 Anirban Nandi, Thomas Chartrand, Werner Van Geit, Anatoly Buchin, Zizhen Yao, Soo Yeun Lee,
487 Yina Wei, Brian Kalmbach, Brian Lee, Ed Lein, et al. Single-neuron models linking electrophys-
488 iology, morphology, and transcriptomics across cortical cell types. *Cell reports*, 40(6), 2022.

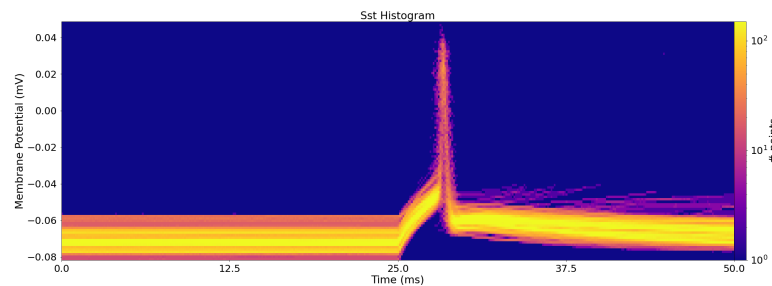
490 Lionel G Nowak, Maria V Sanchez-Vives, and David A McCormick. Lack of orientation and di-
491 rection selectivity in a subgroup of fast-spiking inhibitory interneurons: cellular and synaptic
492 mechanisms and comparison with other electrophysiological cell types. *Cerebral Cortex*, 18(5):
493 1058–1078, 2008.

494 Hiroki Taniguchi, Miao He, Priscilla Wu, Sangyong Kim, Raehum Paik, Ken Sugino, Duda Kvitsani,
495 Yu Fu, Jiangteng Lu, Ying Lin, et al. A resource of cre driver lines for genetic targeting of
496 gabaergic neurons in cerebral cortex. *Neuron*, 71(6):995–1013, 2011.

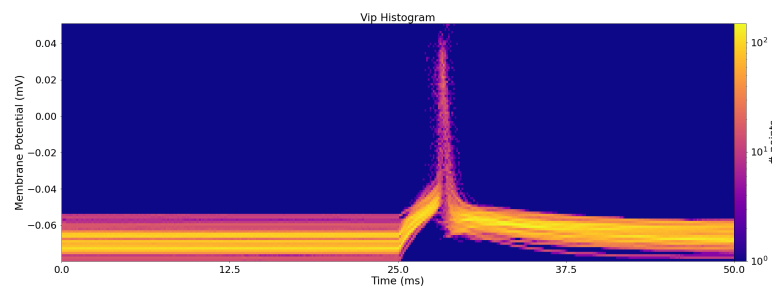
497 Bosiljka Tasic, Zizhen Yao, Lucas T Graybuck, Kimberly A Smith, Thuc Nghi Nguyen, Darren
498 Bertagnolli, Jeff Goldy, Emma Garren, Michael N Economo, Sarada Viswanathan, et al. Shared
499 and distinct transcriptomic cell types across neocortical areas. *Nature*, 563(7729):72–78, 2018.

501 Petilla Interneuron Nomenclature Group; PING and others. Petilla terminology: nomenclature of
502 features of gabaergic interneurons of the cerebral cortex. *Nature reviews. Neuroscience*, 9(7):557,
503 2008.

505 A HISTOGRAMS OF ELECTROPHYSIOLOGY RECORDING DATA



508
509
510
511
512
513
514
515
516
517
518 Figure 5: Time series histogram of the current-clamp electrophysiology recordings for Sst



519
520
521
522
523
524
525
526
527
528
529
530 Figure 6: Time series histogram of the current-clamp electrophysiology recordings for Vip

531
532
533
534
535
536
537
538
539

540
541
542
543
544
545
546
547
548
549
550
551
552
553
554
555
556
557
558
559
560
561
562
563
564
565
566
567
568
569
570
571
572
573
574
575
576
577
578
579
580
581
582
583
584
585
586
587
588
589
590
591
592
593

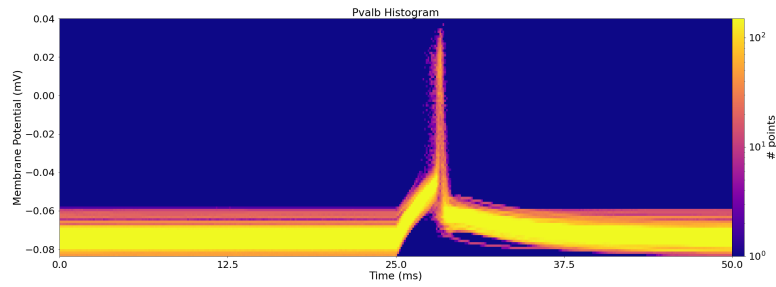


Figure 7: Time series histogram of the current-clamp electrophysiology recordings for Pvalb

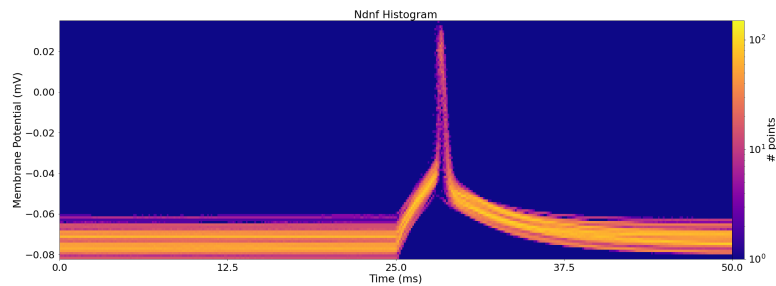


Figure 8: Time series histogram of the current-clamp electrophysiology recordings for Ndnf

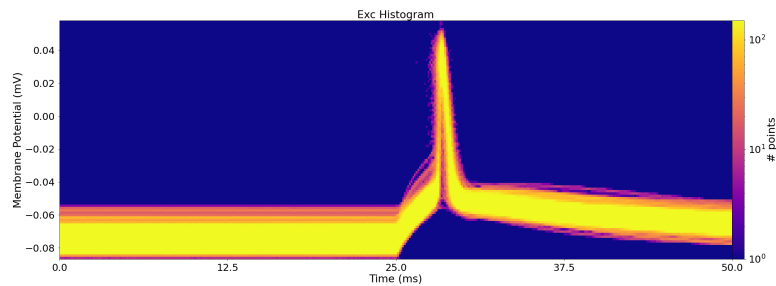


Figure 9: Time series histogram of the current-clamp electrophysiology recordings for Exc

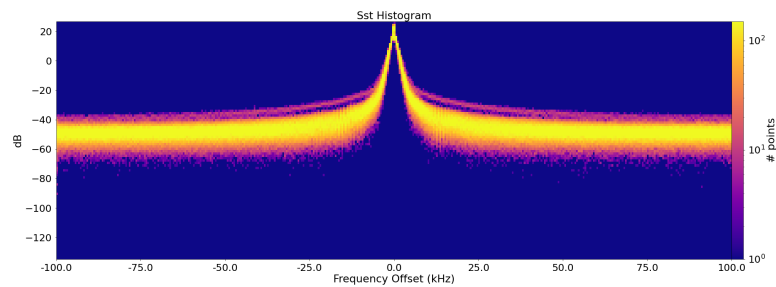


Figure 10: Fourier spectra histogram of the time series data for Sst

594
595
596
597
598
599
600
601
602
603
604
605
606
607
608
609
610
611
612
613
614
615
616
617
618
619
620
621
622
623
624
625
626
627
628
629
630
631
632
633
634
635
636
637
638
639
640
641
642
643
644
645
646
647

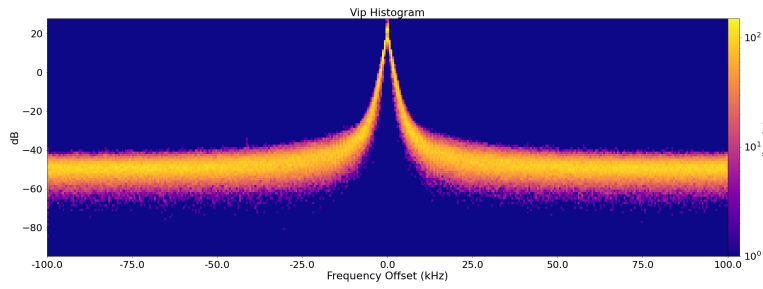


Figure 11: Fourier spectra histogram of the time series data for Vip

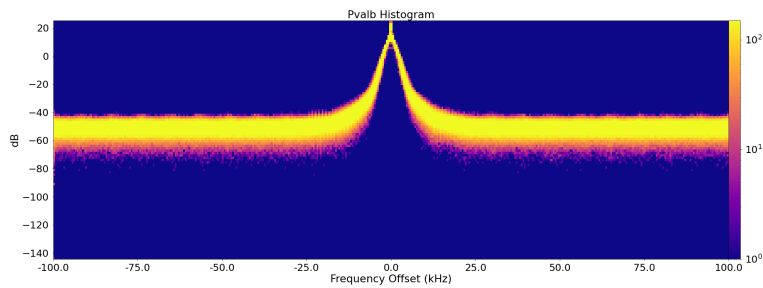


Figure 12: Fourier spectra histogram of the time series data for Pvalb

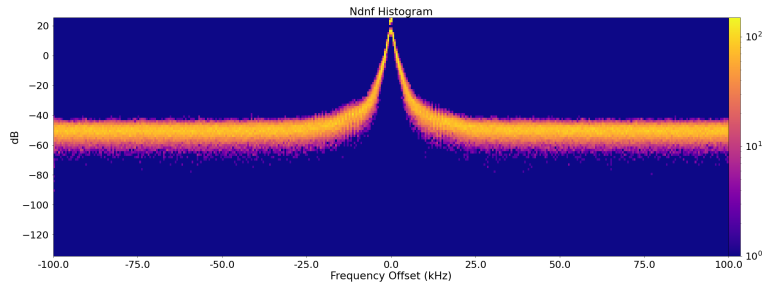


Figure 13: Fourier spectra histogram of the time series data for Ndnf

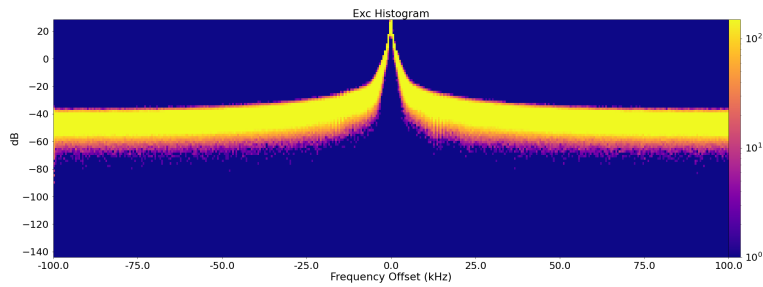


Figure 14: Fourier spectra histogram of the time series data for Exc